APL Materials

Hole-transport material variation in fully vacuum deposited perovskite solar cells

Cite as: APL Mater. **2**, 081503 (2014); https://doi.org/10.1063/1.4889843
Submitted: 28 May 2014 • Accepted: 30 June 2014 • Published Online: 14 July 2014

Lauren E. Polander, Paul Pahner, Martin Schwarze, et al.

APL MATERIALS **2**, 081503 (2014)

Hole-transport material variation in fully vacuum deposited perovskite solar cells

Lauren E. Polander, Paul Pahner, Martin Schwarze, Matthias Saalfrank, Christian Koerner, and Karl Leo[a]
Institut für Angewandte Photophysik, Technische Universität Dresden, 01069 Dresden, Germany

(Received 28 May 2014; accepted 30 June 2014; published online 14 July 2014)

This work addresses the effect of energy level alignment between the hole-transporting material and the active layer in vacuum deposited, planar-heterojunction $CH_3NH_3PbI_{x-3}Cl_x$ perovskite solar cells. Through a series of hole-transport materials, with conductivity values set using controlled p-doping of the layer, we correlate their ionization potentials with the open-circuit voltage of the device. With ionization potentials beyond 5.3 eV, a substantial decrease in both current density and voltage is observed, which highlights the delicate energetic balance between driving force for hole-extraction and maximizing the photovoltage. In contrast, when an optimal ionization potential match is found, the open-circuit voltage can be maximized, leading to power conversion efficiencies of up to 10.9%. These values are obtained with hole-transport materials that differ from the commonly used Spiro-MeO-TAD and correspond to a 40% performance increase *versus* this reference. [http://dx.doi.org/10.1063/1.4889843]

In the last five years, a new class of inorganic–organic photovoltaic (PV) devices based on methylammonium lead halide perovskite absorbers ($CH_3NH_3PbX_3$, X = Br, Cl, I)[1–3] have attracted considerable attention mainly due to three significant advantages: inexpensive precursors, a variety of available fabrication methods,[4] and consistently high power conversion efficiency values.[5,6] Many studies have highlighted the exceptional characteristics of these perovskite materials, which not only exhibit panchromatic absorption, but also display charge-carrier mobility values comparable to amorphous silicon[7] and balanced electron/hole diffusion lengths exceeding 1 μm.[8] These findings prompted the use of organolead trihalide perovskites as a standalone absorber/transport material in planar-heterojunction device architectures,[5,9,10] moving towards standard stacks used in organic PVs,[11–13] with very promising results.

Minimizing energy losses while favoring high charge-extraction rates is fundamental to take greater advantage of the intrinsic properties of the perovskites and achieve efficiencies beyond the current status. Notably, and by analogy from organic PV device theory,[14,15] while the maximum open-circuit photovoltage (V_{OC}) can be approximated by the perovskite energy gap, it can be limited by the relative energy difference between the ionization potential/electron affinity (IP/EA) of the hole-/electron-transporting material (HTM/ETM). In other words, to maximize the V_{OC} while still maintaining favorable charge extraction, the IP/EA values of the chosen HTM/ETM must approach but not exceed/deceed those of the perovskite layer, respectively.

This issue has been raised by Schulz *et al.*[16] when they identified that energy losses of up to 0.4 eV could arise from an IP mismatch between the commonly used Spiro-MeO-TAD HTM (IP = 5.0 eV, Figure 1) and $CH_3NH_3PbI_{x-3}Cl_x$ (IP = 5.4 eV). In solution-processed cells, the alignment between the energy levels of the HTM and the perovskites remains to be addressed despite

[a]karl.leo@iapp.de

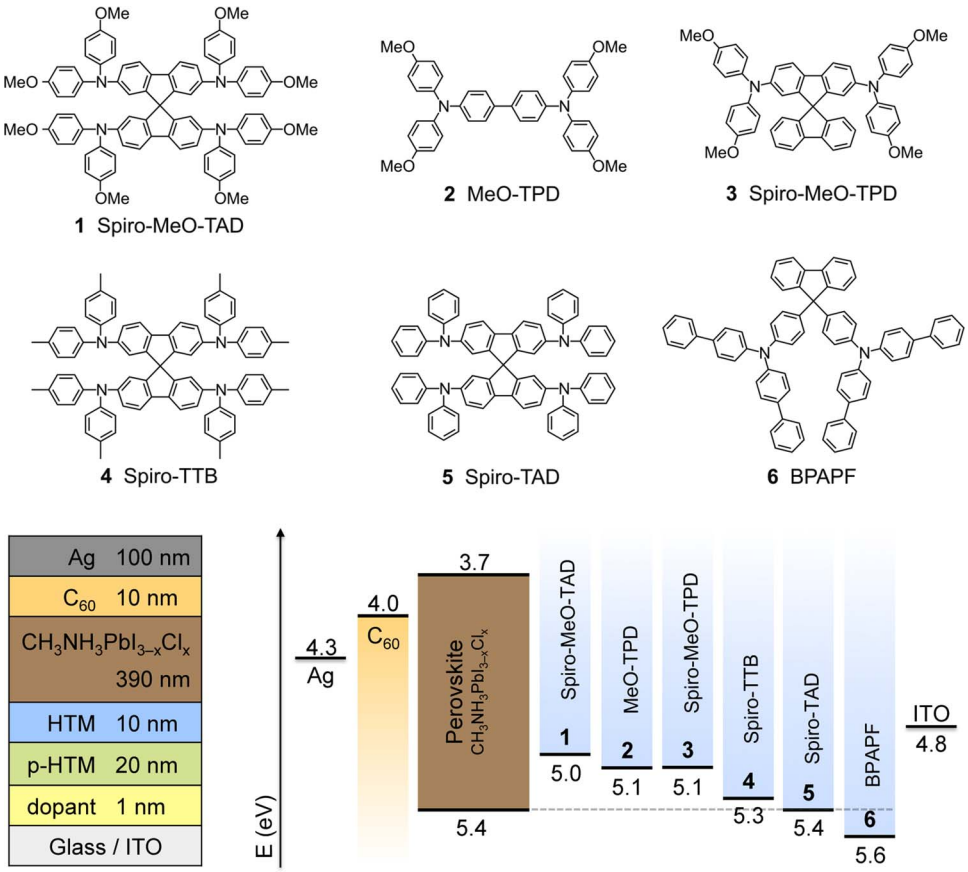

FIG. 1. Chemical structures for the HTMs in this study along with general device architecture and corresponding energy level diagram. Numerical values correspond to the absolute value of the IP and EA as determined by UPS and IPES, respectively. The IP/EA of the perovskite layer and HTM **1** are as reported in Ref. 16.

the exploration of many alternatives (PEDOT:PSS,[11,12] P3HT,[13] poly-triphenylamine derivatives,[11] poly-diketopyrrolopyrrole derivatives,[17] and Spiro-MeO-TAD derivatives[18–20]).

Among recent studies, which have heavily focused on the optimization of solution-processed cells with and without mesoporous metal oxide layers, two reports have identified thin-film vapor deposition as a successful method to fabricate uniform, flat perovskite films[4] and yield high-efficiency devices when used in conjunction with solution-processed transport/blocking materials.[5,11] However, thus far, despite several potential advantages including highly controlled layer deposition, conductivity manipulation using doping techniques,[21] easily varied device architecture, and a diverse library of compatible materials with proven charge-transport characteristics,[22] fully vacuum-processed perovskite PVs have not been investigated.

Herein, we demonstrate the use of $CH_3NH_3PbI_{x-3}Cl_x$ active layers in combination with an industry standard ETM and a variety of vapor-deposited HTMs. This study provides a direct comparison between perovskite and organic PV device architectures, while easily tuning the HTM to minimize energetic losses and improve overall efficiency. Additionally, the relationships identified here are easily transferable and can help guide molecular design of new HTMs in the field of solution-processed perovskite PV.

A standard p–i–n device architecture[23] was chosen for this study consisting of a tin-doped indium oxide (ITO) patterned glass cathode, thin layer of neat p-dopant to improve electrode contact, p-doped hole-transport layer, $CH_3NH_3PbI_{3-x}Cl_x$ perovskite active layer, intrinsic Buckminsterfullerene (C_{60}) electron-transport/hole-blocking layer, and a silver anode (Figure 1). All layers were deposited by thermal evaporation in an ultra-high vacuum chamber. Deposition of the perovskite layer was

TABLE I. Ionization potential[a] determined by ultraviolet photoelectron spectroscopy and short-circuit current density, open-circuit voltage, fill-factor, and power-conversion efficiency values measured under simulated AM 1.5 G sunlight (100 mW cm^{-2}).[b]

HTM	IP_{UPS} (eV)	J_{SC} (mA cm^{-2})	V_{OC} (V)	FF (%)	η (%)
1	5.0	14.4 (14.1 ± 0.5)	795 (820 ± 30)	69 (63 ± 5)	7.8 (7.2 ± 0.5)
2	5.0	14.9 (14.5 ± 0.3)	863 (863 ± 10)	69 (63 ± 7)	8.7 (7.8 ± 1.0)
3	5.1	16.0 (15.5 ± 0.5)	1030 (940 ± 70)	66 (66 ± 3)	10.9 (9.6 ± 0.8)
4	5.3	16.1 (14.9 ± 0.9)	968 (970 ± 30)	70 (63 ± 6)	10.9 (9.1 ± 1.3)
5	5.4	12.4 (12.2 ± 0.5)	820 (815 ± 10)	58 (58 ± 8)	6.7 (5.8 ± 0.8)
6	5.6	0.72	835	13	0.08

[a]Ionization potentials were measured on intrinsic single layers by ultraviolet photoelectron spectroscopy (IP_{UPS} of HTM **1** taken from Ref. 16). Measurement details can be found in the supplementary material.[24]
[b]Average values and standard deviations are based on 8–12 devices fabricated on 3–5 substrates.

achieved *via* dual-source vapor deposition of lead(II) chloride and methylammonium iodide to form the perovskite *in situ* using methods similar to those previously reported.[5,11] Perovskite film formation was confirmed using grazing incidence X-ray diffraction, which also indicated the presence of excess lead halide in the film (e.g., $2\theta = 12^\circ$, Figure S3 of the supplementary material). Incomplete perovskite formation likely led to reduced solar cell performance compared to literature examples (see below); however, particular care was taken to maintain consistent film quality throughout this study, allowing for direct comparison of the HTMs. Further details concerning the evaporation of all materials can be found in the supplementary material.[24]

In addition to the Spiro-MeO-TAD reference (**1**), five other HTMs with increasing IP were chosen for this study (Figure 1): MeO-TPD (**2**, IP = 5.1 eV), Spiro-MeO-TPD (**3**, IP = 5.1 eV), Spiro-TTB (**4**, IP = 5.3 eV), Spiro-TAD (**5**, IP = 5.4 eV), and BPAPF (**6**, IP = 5.6 eV). These materials are in a family of similarly structured triarylamine derivatives whose hole-transport properties are well known from their previous use in the field of Organic Electronics.[22,25] It was expected that maintaining structural similarity would provide minimal effect on other device characteristics, such as morphology, interface compatibility, and mobility. However, to ensure efficient charge transport through the layers, the doping ratio of each material was optimized to maintain relatively consistent conductivity values above 1×10^{-5} S cm^{-1}. Each material was initially tested at 2 wt. % doping of either F_6-TCNNQ (HTMs **1**–**5**) or NDP9 (HTM **6**). In the case of HTMs **5** and **6**, this doping ratio resulted in conductivities well below the range of the other HTMs ($\sigma < 1 \times 10^{-5}$ S cm^{-1}). Therefore, an increased doping ratio of 10 wt. % was used for these materials in order to achieve comparable conductivity values (Figure S5 of the supplementary material).[24]

A diagram depicting the energy levels of each material is provided in Figure 1. The EA value for C_{60} was determined using inverse photoelectron spectroscopy (IPES)[26] and the IP values noted for the $CH_3NH_3PbI_{3-x}Cl_x$ perovskite[16] and HTMs **1**–**6** (Ref. 16) were determined using ultraviolet photoelectron spectroscopy (UPS). HTMs **1**–**6** provide progressively larger IP values approaching and exceeding that of the perovskite layer in order to determine the energetic limit at which the highest V_{OC} and efficiency is achieved without significant adverse losses.

The solar-to-electrical power conversion efficiencies were evaluated by recording the $J-V$ characteristics under simulated AM 1.5 G conditions (100 mW cm^{-2}). Detailed photovoltaic parameters (J_{SC}, V_{OC}, FF, and η) for all materials are reported in Table I and average values with standard deviation for the solar cell characteristics are compared in Figure 2. These values are derived from 8–12 devices fabricated on 3–5 individual substrates *via* identical methods. As expected, while the J_{SC} and FF remain relatively constant for devices employing **1**–**4**, an increase in the IP of the HTM results in greater average V_{OC}, and a corresponding increase in efficiency. However, devices employing HTM **5** show a marked decrease in both J_{SC} and V_{OC}, presumably due to hole extraction difficulties in absence of driving force between the HTM and perovskite layers. The effect is even more pronounced in devices employing HTM **6** (not pictured due to axis scale), where the imposed energy barrier for charge extraction leads to very low efficiency cells.

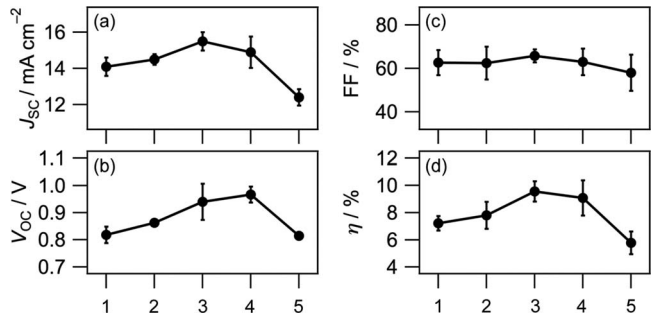

FIG. 2. Average values and standard deviations of the (a) short-circuit current density, (b) open-circuit voltage, (c) fill-factor, and (d) power-conversion efficiency for devices employing HTMs **1**–**5**.

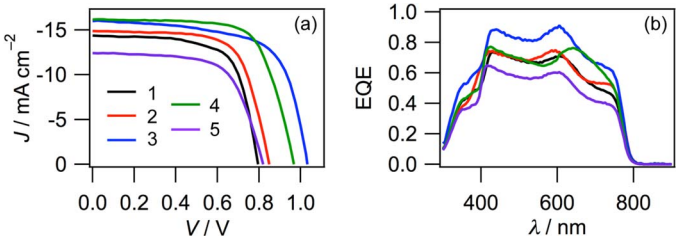

FIG. 3. (a) *J*–*V* characteristics and (b) external quantum efficiency as a function of wavelength measured under simulated AM 1.5 G simulated sunlight (100 mW cm^{-2}) for devices employing HTMs **1**–**5**.

The *J*–*V* characteristics of the best performing cells employing HTMs **1**–**5** are depicted in Figure 3(a) and maintain the trend observed for the average values. The overall highest efficiency devices were obtained using HTMs **3** and **4** with similar J_{SC}, V_{OC}, and FF leading to matched overall power-conversion efficiencies of up to 10.9%. As a consequence of the increased IP, the efficiency of these devices far surpassed that of the device with HTM **1** ($\eta = 7.82\%$) mainly due to an increase in the measured V_{OC} (∼200 mV).

Figure 3(b) shows the external quantum efficiency (EQE) as a function of the light excitation wavelength for devices employing **1**–**5**. The traces are characterized by three main peaks in the 400–800 nm range, with maximum EQE as high as 85%–90%. The spectral response was measured without bias illumination and, for this reason, we did not expect the integration of the curve to exactly match that of the measured J_{SC} for all samples; however, there is a strong correlation to the trend observed for the *J*–*V* characteristics.

Fully vacuum deposited, planar-heterojunction $CH_3NH_3PbI_{x-3}Cl_x$ perovskite solar cells were fabricated in combination with a p-doped hole-transport layer and a C_{60} electron-transport layer. A series of hole-transport materials with ionization potentials ranging from 5.0 to 5.6 eV were investigated to study the influence of improved energy level alignment on the device performance. Devices employing materials with ionization potentials of up to 5.3 eV yielded improved open-circuit voltages, and corresponding power-conversion efficiencies. However, beyond this range, the absence of a driving force for hole-extraction lead to a dramatic decrease in both the short-circuit current density and open-circuit voltage. As such, this work has identified an optimal range for the ionization potential of the hole-transport material in $CH_3NH_3PbI_{x-3}Cl_x$ perovskite solar cells leading to power-conversion efficiency values of up to 10.9%. This corresponds to a 40% improvement over identical devices fabricated with commonly used Spiro-MeO-TAD.

We gratefully acknowledge Dr. Lutz Wilde, Fraunhofer Institut für Photonische Mikrosysteme, Center Nanoelektronische Technologien (IPMS-CNT), for grazing incidence X-ray diffraction measurements.

[1] A. Kojima, K. Teshima, Y. Shirai, and T. Miyasaka, J. Am. Chem. Soc. **131**, 6050 (2009).
[2] J.-H. Im, C.-R. Lee, J.-W. Lee, S.-W. Park, and N.-G. Park, Nanoscale **3**, 4088 (2011).

[3] H. J. Snaith, J. Phys. Chem. Lett. **4**, 3623 (2013).
[4] D. B. Mitzi, Prog. Inorg. Chem. **48**, 1 (1999).
[5] M. Liu, M. B. Johnston, and H. J. Snaith, Nature **501**, 395 (2013).
[6] J. Burschka, N. Pellet, S.-J. Moon, R. Humphry-Baker, P. Gao, M. K. Nazeeruddin, and M. Grätzel, Nature **499**, 316 (2013).
[7] C. Wehrenfennig, G. E. Eperon, M. B. Johnston, H. J. Snaith, and L. M. Herz, Adv. Mater. **26**, 1584 (2014).
[8] S. D. Stranks, G. E. Eperon, G. Grancini, C. Menelaou, M. J. P. Alcocer, T. Leijtens, L. M. Herz, A. Petrozza, and H. J. Snaith, Science **342**, 341 (2013).
[9] G. E. Eperon, V. M. Burlakov, P. Docampo, A. Goriely, and H. J. Snaith, Adv. Funct. Mater. **24**, 151 (2014).
[10] Q. Chen, H. Zhou, Z. Hong, S. Luo, H.-S. Duan, H.-H. Wang, Y. Liu, G. Li, and Y. Yang, J. Am. Chem. Soc. **136**, 622 (2014).
[11] O. Malinkiewicz, A. Yella, Y. Lee, G. Espallargas, M. Grätzel, M. K. Nazeeruddin, and H. J. Bolink, Nat. Photonics **8**, 128 (2014).
[12] J. You, Z. Hong, Y. Yang, Q. Chen, M. Cai, T.-B. Song, C.-C. Chen, S. Lu, Y. Liu, and H. Zhou, ACS Nano **8**, 1674 (2014).
[13] B. Conings, L. Baeten, C. De Dobbelaere, J. D'Haen, J. Manca, and H.-G. Boyen, Adv. Mater. **26**, 2041 (2014).
[14] B. Kippelen and J.-L. Brédas, Energy Environ. Sci. **2**, 251 (2009).
[15] M. Riede, T. Mueller, T. Mueller, W. Tress, R. Schueppel, R. Schueppel, and K. Leo, Nanotechnology **19**, 424001 (2008).
[16] P. Schulz, E. Edri, S. Kirmayer, G. Hodes, D. Cahen, and A. Kahn, Energy Environ. Sci. **7**, 1377 (2014).
[17] Y. S. Kwon, J. Lim, H.-J. Yun, Y.-H. Kim, and T. Park, Energy Environ. Sci. **7**, 1454 (2014).
[18] J. Wang, S. Wang, X. Li, L. Zhu, Q. Meng, Y. Xiao, and D. Li, Chem. Commun. **50**, 5829 (2014).
[19] T. Krishnamoorthy, F. Kunwu, P. Boix, and H. Li, J. Mater. Chem. A **2**, 6305 (2014).
[20] N. J. Jeon, J. Lee, J. H. Noh, M. K. Nazeeruddin, M. Grätzel, and S. I. Seok, J. Am. Chem. Soc. **135**, 19087 (2013).
[21] K. Walzer, B. Maennig, M. Pfeiffer, and K. Leo, Chem. Rev. **107**, 1233 (2007).
[22] Y. Shirota and H. Kageyama, Chem. Rev. **107**, 953 (2007).
[23] B. Maennig, J. Drechsel, D. Gebeyehu, P. Simon, F. Kozlowski, A. Werner, S. Grundmann, S. Sonntag, M. Koch, K. Leo, M. Pfeiffer, H. Hoppe, D. Meissner, N. S. Sariciftci, I. Riedel, V. Dyakonov, and J. Parisi, Appl. Phys. A **79**, 1 (2004).
[24] See supplementary material at http://dx.doi.org/10.1063/1.4889843 for full experimental details.
[25] T. P. I. Saragi, T. Spehr, A. Siebert, T. Fuhrmann-Lieker, and J. Salbeck, Chem. Rev. **107**, 1011 (2007).
[26] W. Zhao and A. Kahn, J. Appl. Phys. **105**, 123711 (2009).